LAWRENCE
LIVERMORE
NATIONAL
LABORATORY

UCRL-JRNL-224375

Combined Plate Motion and Density Driven Flow in the Asthenosphere beneath Saudi Arabia: Evidence from Shearwave Splitting and Seismic Anisotropy

S. Hansen, S. Schwartz, A. Al-Amri, A. Rodgers

September 12, 2006

The Geological Society of America

Publisher: GSA
Journal: GEOL: Geology
Article ID: G22713

Combined Plate Motion and Density Driven Flow in the Asthenosphere beneath Saudi Arabia: Evidence from Shear-wave Splitting and Seismic Anisotropy

Samantha Hansen[1,3]

Susan Schwartz[1]

Abdullah Al-Amri[2]

Arthur Rodgers[3]

[1]*University of California, Santa Cruz, Earth Sciences and IGPP, 1156 High St., Santa Cruz, CA 95064*

[2]*King Saud University, Geology Dept. and Seismic Studies Center, P.O. Box 2455, Riyadh, Saudi Arabia 11451*

[3]*Lawrence Livermore National Laboratory, Energy and Environment Directorate, 7000 East Ave., Livermore, CA 94551*

ABSTRACT

Mantle anisotropy along the Red Sea and across the Arabian Peninsula was analyzed using shear-wave splitting recorded by stations from three different seismic networks: the largest, most widely distributed array of stations examined across the Arabian Peninsula to date. Stations near the Gulf of Aqaba display fast orientations aligned parallel to the Dead Sea Transform Fault, most likely related to the strike-slip motion between Africa and Arabia. However, most of our observations across Arabia are statistically the same (at a 95% confidence level), with north-south oriented fast directions and delay times averaging about 1.4 s. Since end-member models of fossilized anisotropy and present-day asthenospheric flow do not adequately

explain these observations, we interpret them as a combination of plate and density driven flow in the asthenosphere. Combining northeast oriented flow associated with absolute plate motion with northwest oriented flow associated with the channelized Afar upwelling along the Red Sea produces a north-south resultant that matches the observations and supports models of active rifting.

Keywords: Arabia, Red Sea, anisotropy, shear-wave splitting, continental rifting, mantle flow

INTRODUCTION

When deformed by dislocation creep, olivine in the upper mantle develops lattice preferred orientations (LPO), where the crystallographic a-axes [100] become parallel to the induced shear, leading to velocity variations with propagation direction (Mainprice and Silver, 1993). Shear waves encountering such anisotropic regions split into two orthogonal components, one traveling faster than the other. The anisotropy can be characterized by the polarization direction of the fast wave (φ) and the delay time between the fast and slow waves (δt), and these measurements can be used to provide constraints on the mechanisms causing deformation in the upper mantle (Silver and Chan, 1991; Vinnik et al., 1992). In rift environments, one may expect a rift-perpendicular φ since LPO should develop parallel to extension for dry upper mantle conditions (Ribe, 1992). However, in a number of rift environments, such as the Baikal Rift zone, the Rio Grande Rift, and the East African Rift, the observed φ is actually closer to rift-parallel (Gao et al., 1997; Gashawbeza et al., 2004; Walker et al., 2004). This may indicate more complex rifting mechanisms or other deformation processes that dominate extension signatures. It has also been suggested that anisotropy observations may reflect previous tectonic episodes whose anisotropic signature has been "frozen" into the lithosphere (Gashawbeza et al., 2004; Walker et al., 2004).

Saudi Arabia and the Red Sea Rift zone offer an excellent environment in which to study the seismic anisotropy associated with rifting and extension. Several different types of models have been proposed to explain how rifting in the Red Sea developed. The passive rifting model assumes that extensional stresses due to far-field body forces are accommodated on large-scale detachment planes extending through the lithosphere below the rift. This results in passive upwelling of asthenospheric material below the rift, often accompanied by the extrusion of tholeiitic lava (Camp and Roobol, 1992). Flow beneath the rift is parallel to the direction of extension, which would predict a rift-perpendicular φ (Wernicke, 1985; Voggenreiter et al., 1988). The active rifting model involves thermal erosion of the lithosphere by flow in the underlying asthenosphere and requires the presence of hot, ascending material (Camp and Roobol, 1992; Daradich et al., 2003). The rift flanks are thermally uplifted, with elevation decreasing away from the rift axis, and associated lavas have an alkalic composition, reflecting a deep mantle source. Local convection may lead to more complicated flow patterns and therefore more complex anisotropy at depth. Several studies have suggested that these two end-member models may not be mutually exclusive; rifting in the Red Sea may have been initiated by passive processes, followed by more recent active processes associated with a mantle upwelling (Camp and Roobol, 1992; Ebinger and Sleep, 1998; Daradich et al., 2003).

Several previous anisotropy studies near the Red Sea revealed fairly consistent patterns. Analysis of shear-wave splitting from 8 IRIS-PASSCAL stations across western Arabia (Fig. 1), by Wolfe et al. (1999), found δt of 1.0–1.5 s and φ oriented approximately north-south. Receiver function analysis by Levin and Park (2000) found evidence for a more complex anisotropic structure beneath one GSN station, consisting of two dipping layers at depth, but with a resultant φ oriented north-south. Further north, Schmid et al. (2004) and Levin et al. (2006) examined

splitting at several stations near the Gulf of Aqaba and the Dead Sea Transform (DST) Fault, where they found average δt of 1.3 s and φ slightly east of north, with some evidence for a more complex, two-layer anisotropic model. However, each of these studies was somewhat limited in their station distribution and data sampling.

In this study, we present a more comprehensive analysis of the anisotropic signature along the Red Sea and across Saudi Arabia by analyzing shear-wave splitting recorded by stations from three different seismic networks. This is the largest, most widely distributed array of stations examined across Saudi Arabia to date. We demonstrate that the north-south φ is not just valid at isolated sites, but extends throughout the whole of Arabia. These observations cannot be adequately fit by previously proposed models of fossilized anisotropy or present-day absolute plate motion (APM), and we present a new model that consists of a combination of both plate and density driven flow in the asthenosphere.

SHEAR-WAVE SPLITTING ANALYSIS AND RESULTS

Teleseismic data recorded on broadband instruments from three different seismic arrays were used. The largest array, the Saudi Arabian National Digital Seismic Network (SANDSN), includes 25 broadband stations distributed along the eastern edge of the Red Sea and across Saudi Arabia (Fig. 1; Al-Amri and Al-Amri, 1999). SANDSN data from events occurring since 2000 were used for this study. To supplement the SANDSN coverage, we also analyzed data recorded by the 8 IRIS-PASSCAL Saudi Arabian Broadband Array stations, which operated from November 1995 to March 1997 (Vernon and Berger, 1998), as well as data recorded between 1998 and 2001 from 2 stations deployed in Jordan (Rodgers et al., 2003; Fig. 1).

We primarily analyzed SKS phases recorded at these stations, but some S and SKKS phases were also included to improve the incidence angle and back-azimuth coverage. The data

were band-pass filtered between 0.05 and 1 Hz to isolate the shear-wave energy, and measurements of the splitting parameters and their associated errors were made using the approach of Silver and Chan (1991). In total, we used 135 events including 247 SKS phases, 12 SKKS phases, and 52 S phases (see the electronic auxiliary material for details[*]).

Average splitting parameters from different events at each station are shown in Figure 1. Broadly, all stations display a north-south φ with an average δt of 1.4 s, similar to previous findings throughout the area (Wolfe et al., 1999; Levin and Park, 2000). Statistical methods were used to examine the variation in splitting observations at individual stations more closely and to compare the observations from different stations to one another. None of the stations showed significant back-azimuth variation, implying that multiple layers of anisotropy or dipping anisotropic symmetry axes are not required, and the observations at most stations were statistically indistinguishable. Stations near the Gulf of Aqaba (Fig. 1 inset) are a noteable exception. While statistically similar to one another, this group of stations displays a statistically different (at a 95% confidence level) average φ that is rotated further east than the other stations examined.

DISCUSSION

Gulf of Aqaba Stations

Our results in the Gulf of Aqaba region are similar to observations made at nearby stations by Schmid et al. (2004) and Levin et al. (2006). At the two stations they examined, Schmid et al. (2004) found an average φ of 3°-8° east of north and a δt of 1.3 s. They argue that φ is parallel to the DST due to the strike-slip motion between Arabia and Africa. Levin et al. (2006) postulate that their data is better fit by a two-layer model, where neither layer has a φ parallel to the DST. Their interpretation is that the two-layer model reflects deformation in the

asthenosphere caused by APM overlain by fossilized anisotropy. Our observations near the DST can be fit by a two-layer model similar to the one proposed by Levin et al. (2006); however, this fit is not statistically better than our one-layer model given the greater degrees of freedom. Therefore, we conclude that a one-layer model whose φ is parallel to the DST can best explain the splitting observations at the Gulf of Aqaba stations. This concurs with the findings of Schmid et al. (2004) and is similar to anisotropy observations made along other transform boundaries (Vinnik et al., 1992; Bostock and Cassidy, 1995).

Stations across Saudi Arabia

Aside from the Gulf of Aqaba stations, most of the splitting observations across Saudi Arabia are very consistent; yet, a straightforward explanation for these observations is difficult to apply. Wolfe et al. (1999) concluded that the predominantly north-south φ reflects either fossilized anisotropy or present-day asthenospheric flow. We believe that neither of these end-member models adequately fit the observations. A majority of the examined stations are located on the Arabian Shield, an area composed of Proterozoic terranes that mostly strike north-south (Fig 2; Stoeser and Camp, 1985). Therefore, the splitting observed at these stations might be attributed to fossilized structure associated with the convergence of these terranes during the Shield's assembly. However, post-accretionary tectonics produced the northwest trending, strike-slip Najd fault zone, which has had 200-300 km of displacement (Fig. 2; Stoeser and Camp, 1985). Therefore, it seems unlikely that anisotropy imparted during Proterozoic assembly of the Arabian Shield was not disturbed by more recent deformation. For stations on the Arabian Platform (Fig. 2), there is little geologic constraint on any potential fossilized anisotropy since the Proterozoic basement is covered by a thick layer of Phanerozoic sediments (Stoeser and Camp, 1985).

Fossilized anisotropy can also be constrained by lithospheric thickness. Using common percentages of anisotropy (4-5%; Mainprice and Silver, 1993), the lithosphere beneath Saudi Arabia would need to be about 140 km thick to accumulate the observed δt. Although sparse in this region, estimates of lithospheric thickness have been determined with seismic refraction and receiver function methods and are 100-120 km near the Shield-Platform boundary (Mooney et al., 1985) and 80-100 km within the Shield (Sandvol et al., 1998). Closer to the Red Sea, xenolith and isotope studies indicated that the lithosphere thins to as little as 40 km (Altherr et al., 1990; Camp and Roobol, 1992). This substantial thinning is corroborated by seismic waveform modeling, P-wave tomography, and Sn attenuation studies in western Arabia (Rodgers et al., 1999; Benoit et al., 2003; Al-Damegh et al., 2004). Therefore, the lithosphere is probably not thick enough, especially near the Red Sea Rift, to generate the δt observed. In addition, since the lithosphere thins from the Shield to the Red Sea, fossilized anisotropy should produce a pattern of increasing δt at stations from west to east. No such pattern exists, and instead our δt values across Saudi Arabia are remarkably consistent (Fig. 1), casting further doubt on fossilized anisotropy as a viable model for this region.

An alternative explanation for the observed splitting is the alignment of φ with APM due to shear at the base of the lithosphere. Several estimates of the APM for Arabia have been proposed using a variety of global plate models. Gripp and Gordon's (2002) HS3-NUVEL1A model produces an APM direction for Arabia of about N55°W. However, their model is based only on western hemisphere hotspots and does not fit African hotspots well. Therefore, this model probably does not provide the best estimate for Arabian APM. Instead, Global Positioning System (GPS) plate models indicate that Arabia is moving northeast, with an average rate and direction of 22 mm/yr and N40°E, respectively (Reilinger et al., 1997; Sella et al., 2002;

McClusky et al., 2003). The GPS results are comparable to Wolfe et al.'s (1999) APM calculation, based on the O'Conner and le Roex (1992) African APM model. When compared to the GPS-determined APM direction, the orientation of φ is at least 30° different; therefore, this explanation also fails to fit the observations.

Since the end-member models discussed above do not fit the splitting observations, we conclude that the anisotropy is the result of an interaction of mantle flow in the asthenosphere. Shear caused by APM, directed approximately N40°E at 22 mm/yr (Reilinger et al., 1997; McClusky et al., 2003), may affect the alignment of mantle minerals. However, based on variations in the topography and the distribution of alkalic volcanics, it has also been suggested that flow radiating from the Afar mantle upwelling is channelized towards the Red Sea Rift (Camp and Roobol, 1992; Ebinger and Sleep, 1998), in a direction oriented at about N30°W. Assuming that the strain caused by this upwelling is comparable to that caused by plate motion, we can combine these two flow orientations, similar to the vector approach of Silver and Holt (2002), to obtain a north-south oriented resultant (Fig. 3).

Several other lines of evidence also help support our conclusions. Seismic tomography models show that the upper mantle beneath western Arabia is anomalously slow, with velocities increasing toward the continental interior (Debayle et al., 2001; Benoit et al., 2003). These observations are attributed to thermal differences and indicate much hotter mantle beneath the Red Sea, consistent with flow directed beneath the Rift. Daradich et al. (2003) demonstrated that the higher elevations along the Red Sea and the overall tilt of the Arabian plate result from viscous stresses associated with large-scale mantle flow from the Afar upwelling. Walker et al. (2005) compared splitting results from both Wolfe et al. (1999) in Saudi Arabia and Gashawbeza et al. (2004) in Ethiopia to the parabolic asthenospheric flow model expected from a plate

moving over a stationary hotspot. Over 90% of the splitting observations are consistent with radial flow, and they attribute the remaining variations to flow modifying factors, such as channelization by topography at the base of the lithosphere. In addition, Schilling et al. (1992) found isotopic evidence for mantle mixing between depleted asthenosphere and plume flow in Saudi Arabia, supporting the idea of flow interaction at depth. This combination of both plate and density driven flow explains the consistent anisotropic signature across Saudi Arabia. Additionally, the rift-oblique φ, the higher topography, and the presence of alkalic lava extrusions near the Red Sea Rift are all consistent with an active rifting model.

CONCLUSIONS

Teleseismic shear-wave splitting along the Red Sea and across Saudi Arabia reveals that stations in the Gulf of Aqaba display φ aligned parallel to the DST. The remaining observations across Saudi Arabia show a consistent north-south φ with δt averaging 1.4 s. Present-day plate motion does not match the observed φ orientation, and lithospheric thickness constraints indicate that fossilized anisotropy cannot explain the observed δt. Therefore, we interpret the anisotropic signature as a combination of plate and density driven flow in the asthenosphere. Combining the northeast oriented flow associated with APM with the northwest oriented flow associated with the channelized Afar upwelling generates a north-south oriented resultant that matches our splitting observations. Other evidence supporting channelized flow is also consistent with active rifting processes.

ACKNOWLEDGMENTS

We thank the Incorporated Research Institutions for Seismology for providing PASSCAL data, Vadim Levin and Hrvoje Tkalčić for several helpful discussions, and Eric Sandvol, Kris Walker, and an anonymous reviewer for their thorough critiques of this manuscript. This work

was supported by the Institute of Geophysics and Planetary Physics and was performed in part under the auspices of the U.S. Department of Energy by University of California Lawrence Livermore National Laboratory under contract No. W-7405-Eng-48. UCRL-JRNL-218810.

REFERENCES CITED

Al-Amri, M., and Al-Amri, A., 1999, Configuration of the Seismographic Networks in Saudi Arabia: Seismological Research Letters, v. 70, p. 322–331.

Al-Damegh, K., Sandvol, E., Al-Lazki, A., and Barazangi, M., 2004, Regional seismic wave propagation (Lg and Sn) and Pn attenuation in the Arabian Plate and surrounding regions: Geophysical Journal International, v. 157, p. 775-795.

Altherr, R., Henjes-Kunst, F., Puchelt, H., and Baumann, A., 1990, Volcanic activity in the Red Sea axial trough-Evidence for a large mantle diaper: Tectonophysics, v. 150, p. 121-133.

Benoit, M., Nyblade, A., VanDecar, J., and Gurrola, H., 2003, Upper mantle P wave velocity structure and transition zone thickness beneath the Arabian Shield: Geophysical Research Letters, v. 30, doi:10.1029/2002GL016436.

Bostock, M., and Cassidy, J., 1995, Variations in SKS splitting across western Canada: Geophysical Research Letters, v. 22, p. 5–8, doi:10.1029/94GL02789.

Camp, V., and Roobol, M., 1992, Upwelling Asthenosphere Beneath Western Arabia and Its Regional Implications: Journal of Geophysical Research, v. 97, p. 15,255–15,271.

Daradich, A., Mitrovica, J., Pysklywec, R., Willett, S., and Forte, A., 2003, Mantle flow, dynamic topography, and rift-flank uplift of Arabia: Geology, v. 31, p. 901–904, doi:10.1130/G19661.1.

Debayle, E., Lévêque, J., and Cara, M., 2001, Seismic evidence for a deeply rooted low-velocity anomaly in the upper mantle beneath the northeastern Afro/Arabian continent: Earth and Planetary Science Letters, v. 193, p. 423–436, doi:10.1016/S0012-821X(01)00509-X.

Ebinger, C., and Sleep, N., 1998, Cenozoic magmatism throughout east Africa resulting from impact of a single plume: Nature, v. 395, p. 788–791, doi:10.1038/27417.

Gao, S., Davis, P., Liu, H., Slack, P., Rigor, A., Zorin, Y., Mordvinova, V., Kozhevnikov, V., and Logatchev, N., 1997, SKS splitting beneath continental rift zones: Journal of Geophysical Research, v. 102, p. 22,781–22,797, doi:10.1029/97JB01858.

Gashawbeza, E., Klemperer, S., Nyblade, A., Walker, K., and Keranen, K., 2004, Shear-wave splitting in Ethiopia: Precambrian mantle anisotropy locally modified by Neogene rifting: Geophysical Research Letters, v. 31, doi:10.1029/2004GL020471.

Gripp, A., and Gordon, R., 2002, Young tracks of hotspots and current plate velocities: Geophysical Journal International, v. 150, p. 321-361.

Levin, V., and Park, J., 2000, Shear zones in the Proterozoic lithosphere of the Arabian Shield and the nature of the Hales discontinuity: Tectonophysics, v. 323, p. 131–148, doi:10.1016/S0040-1951(00)00105-0.

Levin, V., Henza, A., Park, J., and Rodgers, A., 2006, Texture of mantle lithosphere along the Dead Sea Rift: recently imposed or inherited?: Physics of the Earth and Planetary Interiors, (in press).

Mainprice, D., and Silver, P., 1993, Interpretation of SKS-waves using samples from the subcontinental lithosphere: Physics of the Earth and Planetary Interiors, v. 78, p. 257–280, doi:10.1016/0031-9201(93)90160-B.

McClusky, S., Reilinger, R., Mahmoud, S., Ben Sari, D., and Tealeb, A., 2003, GPS constraints of Africa (Nubia) and Arabia plate motions: Geophysical Journal International, v. 155, p. 126-138.

Mooney, W., Gettings, M., Blank, H., and Healy, J., 1985, Saudi Arabian seismic refraction profile: A traveltime interpretation of crustal and upper mantle structure: Tectonophysics, v. 111, p. 173-246.

O'Conner, J., and le Roex, A., 1992, South Atlantic hot spot-plume systems: 1. Distribution of volcanism in time and space: Earth and Planetary Science Letters, v. 113, p. 343-364.

Reilinger, R., McClusky, S., Oral, M., King, R., Toksoz, M., Barka, A., Kinik, I., Lenk, O., and Sanli, I., 1997, Global Positioning System measurements of present-day crustal movements in the Arabia-Africa-Eurasia plate collision zone: Journal of Geophysical Research, v. 102, p. 9,983–10,000.

Ribe, N., 1992, On the relation between seismic anisotropy and finite strain: Journal of Geophysical Research, v. 97, p. 8,737-8,747.

Rodgers, A., Walter, W., Mellors, R., Al-Amri, A., and Zhang, Y., 1999, Lithospheric structure of the Arabian Shield and Platform from complete regional waveform modeling and surface wave group velocities: Geophysical Journal International, v. 138, p. 871-878..

Rodgers, A., Harris, D., Ruppert, S., Lewis, J., O'Boyle, J., Pasyanos, M., Abdallah, A., Al-Yazjeen, T., and Al-Gazo, A., 2003, A Broadband Seismic Deployment in Jordan: Seismological Research Letters, v. 74, p. 374–381.

Sandvol., E., Seber, D., Barazangi., M., Vernon., F., Mellors, R., and Al-Amri, A., 1998, Lithospheric seismic velocity discontinuities beneath the Arabian Shield: Geophysical Research Letters, v. 25, p. 2,873-2,876.

Schilling, J., Kingsley, R., Hanan, B., and McCully, B., 1992, Nd-Sr-Pb isotopic variations along the Gulf of Aden: evidence for Afar mantle plume – continental lithosphere interaction: Journal of Geophysical Research, v. 97, p. 10,927–10,966.

Schmid, C., van der Lee, S., and Giardini, D., 2004, Delay times and shear wave splitting in the Mediterranean region: Geophysical Journal International, v. 159, p. 275–290, doi:10.1111/j.1365-246X.2004.02381.x.

Sella, G., Dixon, T., and Mao., A., 2002, REVEL: A model for recent plate velocities from space geodesy: Journal of Geophysical Research, v. 107, doi:10.1029/2000JB000033.

Silver, P., and Chan, W., 1991, Shear Wave Splitting and Subcontinental Mantle Deformation: Journal of Geophysical Research, v. 96, p. 16,429–16,454.

Silver, P., and Holt, W., 2002, The Mantle Flow Field Beneath Western North America: Science, v. 295, p. 1,054–1,057.

Stoeser, D., and Camp, V., 1985, Pan-African microplate accretion of the Arabian Shield: Geological Society of America Bulletin, v. 96, p. 817–826, doi:10.1130/0016-7606(1985)96<817:PMAOTA>2.0.CO;2.

Vernon, F., and Berger, J., 1998, Broadband seismic characterization of the Arabian Shield: Final Scientific Technical Report, Department of Energy Contract No. F 19628–95-K-0015, p. 36.

Vinnik, L., Makeyeva, L., Milev, A., and Usenko, A., 1992, Global patterns of azimuthal anisotropy and deformations in the continental mantle: Geophysical Journal International, v. 111, p. 433–447.

294 Voggenreiter, W., Hötzl, H., and Jado, A., 1988, Red Sea related history of extension and
295 magmatism in the Jizan area (Southwest Saudi Arabia): indication for simple-shear during
296 Red Sea rifting: Geologische Rundschau, v. 77, p. 257–274, doi:10.1007/BF01848688.
297 Walker, K., Nyblade, A., Klemperer, S., Bokelmann, G., and Owens, T., 2004, On the
298 relationship between extension and anisotropy: Constraints from shear wave splitting across
299 the East African Plateau: Journal of Geophysical Research, v. 109,
300 doi:10.1029/2003JB002866.
301 Walker, K., Bokelmann, G., Klemperer, S., and Nyblade, A., 2005, Shear wave splitting around
302 hotspots: Evidence for upwelling-related mantle flow?: Geological Society of America
303 Special Paper 388, p. 171-192.
304 Wernicke, B., 1985, Uniform-sense normal simple-shear of the continental lithosphere: Canadian
305 Journal of Earth Sciences, v. 22, p. 108–125. Wolfe, C., Vernon, F., and Al-Amri, A., 1999,
306 Shear-wave splitting across western Saudi Arabia: The pattern of upper mantle anisotropy at
307 a Proterozoic shield: Geophysical Research Letters, v. 26, p. 779–782.
308 Wolfe, C., Vernon, F., and Al-Amri, A., 1999, Shear-wave splitting across western Saudi Arabia:
309 The pattern of upper mantle anisotropy at a Proterozoic shield: Geophysical Research
310 Letters, v. 26, p. 779-782.
311 FIGURE CAPTIONS
312 **Figure 1.** Map showing average splitting parameters. The bold, center lines at each station are
313 oriented in the station's average φ and the length of the line is scaled to the average δt. The
314 dashed "fans" show one standard deviation of the fast angle. The inset provides a closer view of
315 the Gulf of Aqaba stations (gray box). Triangles: SANDSN stations, squares: PASSCAL

stations, circles: Jordon stations. The black arrow shows the average APM direction based on GPS models (Reilinger et al., 1997; McClusky et al., 2003).

Figure 2. Topographic map with geologic boundaries. The boundary between the Arabian Shield (AS) and the Arabian Platform (AP) is marked by the solid bold line, and the approximate location of the Afar upwelling is enclosed by the dashed black circle. The thin dashed lines show the trend of the Najd fault zone, and the thin solid lines show the boundaries of major terranes, whose names are listed. Modified from Stoeser and Camp (1985).

Figure 3. Vector examination of plate motion (white arrow) coupled with channelized upwelling flow (solid black arrow) beneath Saudi Arabia. If we estimate that the APM is oriented N40ºE at a rate of 22 mm/yr (Reilinger et al., 1997; McClusky et al., 2003) and that the channelized hotspot flow is oriented approximately N30ºW (Camp and Roobol, 1992; Ebinger and Sleep, 1998), then the rate of hotspot flow needed to obtain a north-south resultant (black dashed arrow) is about 27 mm/yr.

*GSA Data Repository item 2006xxx, Shear-wave splitting analysis, is available online at www.geosociety.org/pubs/ft2006.htm, or on request from editing@geosociety.org or Documents Secretary, GSA, P.O. Box 9140, Boulder, CO 80301, USA.

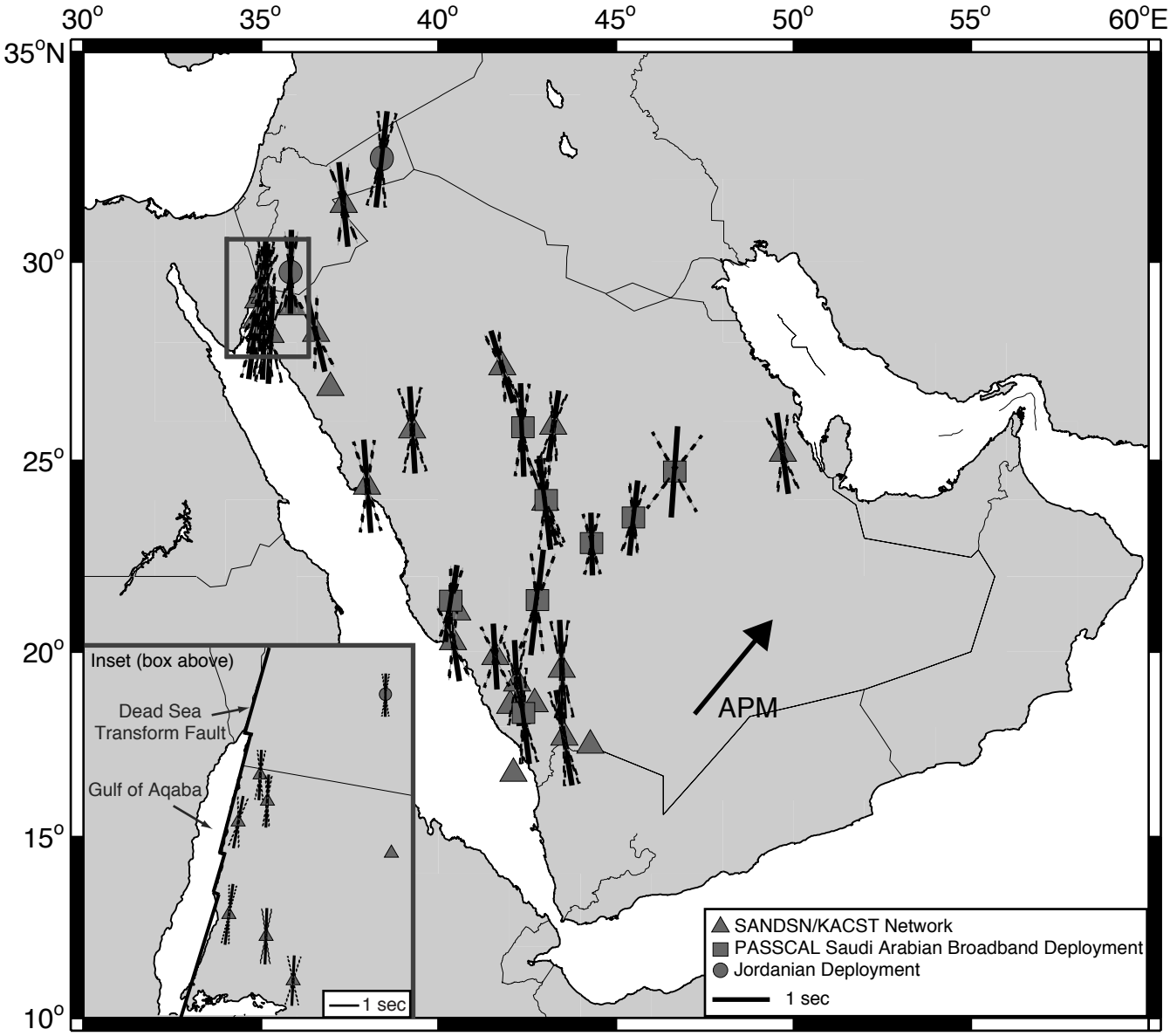

Samantha Hansen
MS#G22713
Figure 1

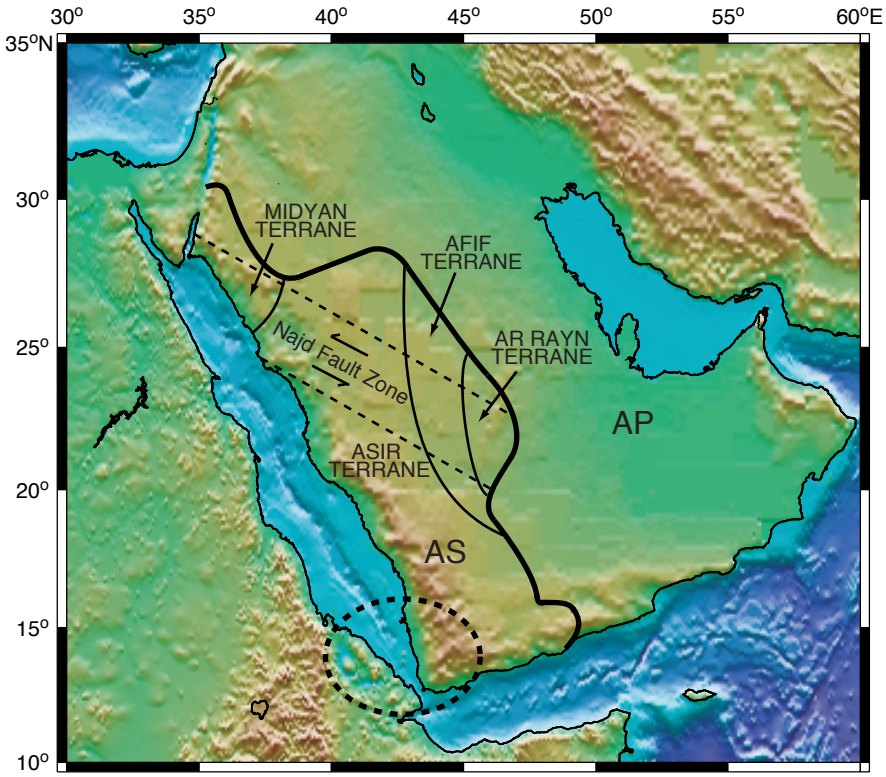

Samantha Hansen
MS#G22713
Figure 2

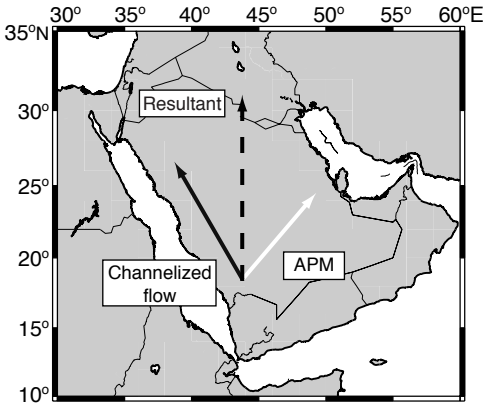

Samantha Hansen
MS#G22713
Figure 3

DATA REPOSITORY ITEM

The following auxiliary material includes:

Table DR1. Events used in the shear-wave splitting study. The ID number of each event used is given along with the corresponding year, Julian day, time, latitude, longitude, depth, and magnitude.

Table DR2. Individual splitting parameters. For each event examined at each corresponding station, this table lists the fast polarization direction (φ) and its associated error, the delay time (δt) and its associated error, and the phase examined.

Table DR3. Average splitting parameters. This table lists the latitude and longitude of each station as well as the average splitting parameter values and their corresponding standard deviations. These values were plotted in Figure 1.

Figure DR1. Map of stations. Stations from three different seismic networks were used in this study. The blue triangles are the broadband stations of the Saudi Arabian National Digital Seismic Network (SANDSN), the yellow triangles are the PASSCAL Saudi Arabian Broadband Array, and the red triangles are the two stations in Jordon. The corresponding names for each station are listed.

Figure DR2. Map of events. The green dots are all of the earthquakes used in this study. The concentric circles mark the distance of the events from the middle of the Saudi Arabian stations (black triangle) in 30° increments. These are the same events from Table DR1.

Figure DR3. Example of shear-wave splitting correction. (a) Original (left) and corrected (right) horizontal waveforms highlighting the SKS arrival from event 1472424 recorded at SANDSN station BDAS. Note that both the radial (top) and transverse (bottom) components show SKS energy on the original waveform, but once corrected, the transverse signal is minimized. (b) Original (left) and corrected (right) particle motion plots for the same event. On the original plot, elliptical particle motion is observed, but on the corrected, the particle motion is linear. (c) Error plot associated with the final solution. The black star marks the parameters that best correct for the splitting. ($\varphi = 10° \pm 4°$, $\delta t = 1.5$ s $\pm$ 0.05 s) and the closest contour is the 95% confidence interval, indicating that the solution is well constrained.

Figure DR4. Hemispherical plots for two SANDSN stations: Gulf of Aqaba station TAYS and Arabian Shield station NAMS. Each line displays the splitting parameters for one event, where the line is oriented in the fast polarization direction (φ) and is scaled to the delay time (δt). The angles on the perimeter show the back-azimuth at which the arrivals are coming from. Black lines correspond to SKS phases, red lines correspond to SKKS phases, and blue lines correspond to S phases. One can see that while observations at station TAYS are rotated further east, neither station shows any variation in the splitting parameters with back-azimuth.

DATA REPOSITORY ITEM

Table DR1. Events used in the shear-wave splitting study

Event ID	Year	Julian Day	Time	Latitude	Longitude	Depth (km)	Magnitude
000512	2000	133	18:43:18	-23.55	-66.45	225	6.2
010705	2001	186	13:53:48	-16.09	-73.99	62	6.2
021012	2002	285	20:09:11	-8.30	-71.74	534	6.5
021112	2002	316	1:46:49	-56.55	-27.54	120	6.0
050613	2005	164	22:44:34	-19.99	-69.20	116	6.8
714489	1995	359	4:43:24	-6.90	129.15	142	6.3
714751	1995	364	2:07:18	63.21	-150.61	137	5.5
714828	1995	365	7:26:12	53.83	160.45	44	6.0
715737	1996	10	22:36:03	-6.13	133.56	38	5.9
717753	1996	46	0:45:54	51.25	-179.41	33	5.6
717994	1996	48	14:21:22	-0.57	135.84	19	5.8
718052	1996	48	20:18:07	-0.92	136.23	32	6.0
718511	1996	53	14:59:09	45.26	148.54	124	6.3
719689	1996	79	17:12:43	15.85	-97.31	33	5.8
720054	1996	87	20:52:07	11.78	-87.93	33	5.5
720100	1996	88	19:51:08	52.31	-168.78	33	5.7
720105	1996	88	21:32:50	52.29	-168.76	33	5.6
720110	1996	88	23:03:50	-1.04	-78.74	33	5.8
720171	1996	90	13:05:17	52.21	-168.73	33	5.9
720923	1996	110	0:19:31	-23.94	-70.09	50	6.0
721264	1996	120	14:40:41	-6.52	155.00	44	6.3
721404	1996	123	13:34:29	-4.55	154.83	500	5.6
721507	1996	125	16:49:25	13.86	146.26	33	5.5
722399	1996	151	3:04:38	-56.72	-26.31	84	5.7
722782	1996	160	23:19:15	51.49	-178.13	33	5.9
722827	1996	162	4:03:35	51.56	-177.63	33	6.6
722931	1996	162	15:24:56	51.48	-176.85	26	5.9
723086	1996	164	2:16:48	51.42	-178.21	33	5.5
723739	1996	178	3:22:03	27.73	139.75	469	5.5
723955	1996	182	11:32:36	51.73	159.81	33	5.5
724135	1996	186	11:39:40	61.85	-150.83	55	5.6

724225	1996	188	21:36:29	21.97	142.83	241	5.8
724503	1996	197	16:51:22	18.73	145.63	177	5.9
724508	1996	197	21:23:34	17.60	-100.97	18	5.7
724537	1996	198	10:07:37	1.02	120.25	33	6.0
725459	1996	218	21:39:16	-2.00	-81.00	33	5.7
726020	1996	232	4:19:16	51.45	-178.37	33	5.7
726575	1996	246	20:41:53	12.32	143.81	33	5.7
726645	1996	248	19:06:50	9.37	-84.27	33	5.8
727822	1996	272	14:10:42	10.04	125.37	235	5.6
728015	1996	276	9:48:02	11.76	125.48	33	6.0
728981	1996	298	19:31:54	66.99	-173.23	20	6.0
731866	1996	357	14:53:28	43.21	138.92	227	6.0
732743	1997	11	20:28:26	18.22	-102.76	33	6.5
732928	1997	16	21:41:07	18.10	-102.68	28	5.6
732949	1997	17	11:20:22	-8.90	123.54	111	6.2
733206	1997	23	2:15:23	-22.00	-65.72	276	6.4
734243	1997	46	12:11:15	-7.78	117.41	274	5.6
757685	1998	141	5:34:26	0.21	119.58	33	6.2
763405	1998	245	8:37:30	5.41	126.76	50	6.6
766330	1998	301	16:25:04	0.84	125.97	33	6.2
960819	1996	232	4:19:16	51.45	-178.37	33	5.7
970720	1997	201	10:14:23	-22.98	-66.30	256	5.7
970727	1997	208	5:21:29	-30.52	-71.86	33	5.8
971217	1997	351	4:38:51	51.19	178.87	20	6.5
971222	1997	356	2:05:50	-5.50	147.87	179	6.3
980130	1998	30	12:16:09	-23.91	-70.21	42	6.5
1321048	1999	312	16:45:43	36.52	71.24	228	6.2
1323924	2000	8	16:47:21	-16.92	-174.25	183	6.5
1325258	2000	37	11:33:52	-5.84	150.88	33	6.6
1326192	2000	57	8:11:48	13.80	144.78	132	6.0
1327281	2000	81	5:26:08	3.16	128.03	103	6.1
1327660	2000	88	11:00:23	22.34	143.73	127	6.8
1329072	2000	112	4:35:18	51.42	-178.14	33	6.0
1329189	2000	114	9:27:23	-28.31	-62.99	609	6.6
1330394	2000	133	18:43:18	-23.55	-66.45	225	6.2
1330404	2000	133	23:10:30	35.97	70.66	108	6.2

1378170	2000	158	9:58:07	-5.09	102.70	33	5.8
1378658	2000	166	17:00:48	4.54	127.72	90	6.1
1378782	2000	168	7:55:35	-33.88	-70.09	120	6.2
1380219	2000	189	15:46:45	51.41	179.98	31	6.4
1380389	2000	192	9:58:19	46.83	145.42	360	6.1
1380392	2000	192	10:39:39	-4.47	103.76	105	5.8
1380430	2000	193	1:32:29	57.37	-154.21	44	6.3
1380683	2000	195	15:50:35	49.45	155.77	81	5.5
1380967	2000	199	22:53:47	36.28	70.92	141	6.0
1381176	2000	202	18:39:19	36.51	140.98	47	6.1
1381291	2000	204	20:56:12	-4.07	102.37	69	5.8
1382400	2000	219	7:27:13	28.86	139.56	395	6.3
1382484	2000	220	14:33:56	-7.02	123.36	649	6.5
1383781	2000	240	17:19:07	22.22	143.76	100	5.6
1383822	2000	241	15:05:48	-4.11	127.39	16	6.5
1383840	2000	241	19:29:25	-4.16	127.31	33	6.0
1383841	2000	241	19:29:32	-4.12	127.03	33	6.5
1385516	2000	270	16:49:33	1.12	127.44	142	5.8
1441489	1998	148	15:20:14	-8.02	114.64	33	6.9
1467240	2000	299	9:32:24	-6.55	105.63	38	6.3
1467351	2000	301	4:21:52	26.27	140.46	388	6.1
1467512	2000	303	8:37:09	-4.77	153.95	50	6.1
1469289	2000	323	6:54:58	-5.23	151.77	33	6.2
1470597	2000	338	12:55:17	51.67	-178.16	43	5.6
1470690	2000	340	11:08:25	4.22	126.44	101	5.5
1471587	2000	354	13:11:47	11.77	144.76	33	6.3
1471662	2000	355	9:19:50	53.42	159.84	67	5.5
1471801	2000	357	10:13:01	44.79	147.20	140	6.0
1472246	2001	9	16:49:28	-14.93	167.17	103	6.3
1472392	2001	13	17:33:32	13.05	-88.66	60	6.4
1472424	2001	14	8:58:25	22.09	143.75	87	5.8
1473169	2001	32	18:19:30	51.44	-177.80	33	5.6
1494829	2000	321	7:42:25	-5.30	153.28	0	6.3
1551781	2001	47	5:59:09	-7.16	117.49	521	5.9
1552135	2001	52	15:22:21	-4.90	102.45	33	5.7
1552306	2001	55	7:23:49	1.27	126.25	35	6.6

1554837	2001	99	9:00:57	-32.67	-73.11	11	6.1
1562488	2001	145	5:06:11	-7.87	110.18	143	5.8
1580135	2002	10	11:14:57	-3.21	142.43	11	6.0
1581565	2002	32	21:55:21	45.46	136.72	356	6.2
1582417	2002	62	12:08:08	36.43	70.44	209	6.3
1589036	2002	87	4:56:22	-21.66	-68.33	125	6.1
1590598	2002	108	16:08:37	-27.54	-70.59	62	6.2
1591203	2002	116	16:06:07	13.09	144.62	86	6.5
1592364	2002	148	4:04:23	-28.94	-66.80	22	6.0
3991464	2002	205	3:05:06	-9.29	118.62	29	5.8
3991754	2002	212	0:16:45	7.93	-82.79	10	6.0
3992367	2002	226	13:57:52	14.10	146.20	30	6.1
4062674	2000	37	11:33:57	-5.93	150.91	72	6.6
4078622	2000	88	11:00:23	22.34	143.73	127	6.8
4205566	2002	277	19:05:49	-20.99	-179.02	621	6.1
4207220	2002	297	21:53:43	6.03	94.42	65	6.2
4208653	2002	316	1:46:49	-56.55	-27.54	120	6.0
4259018	2001	38	15:14:57	55.79	162.76	33	6.0
4268963	2001	59	18:55:01	51.20	-117.20	10	6.6
4351768	2000	133	18:43:21	-22.66	-67.05	224	6.7
4405407	2003	272	16:02:46	48.28	153.17	118	5.5
4409772	2003	301	21:48:21	43.84	147.75	65	6.1
4473144	2002	16	23:10:19	22.50	-93.20	80	6.1
4473481	2002	30	8:42:31	24.40	-95.60	120	6.0
4474575	2002	70	1:46:30	34.80	144.10	10	6.0
4540559	2004	153	3:08:48	34.49	141.39	18	5.2
4567778	2004	316	10:02:47	42.14	144.34	33	5.9
4589463	2004	362	20:10:51	2.93	95.61	29	5.7
4589632	2004	364	13:20:29	28.92	130.44	38	5.5
4590172	2005	6	0:56:30	5.32	94.84	50	6.1
4595874	2005	69	0:28:26	85.25	92.90	10	5.0
4596577	2005	80	16:14:39	-1.06	-24.59	22	5.1

DATA REPOSITORY ITEM

Table DR2. Individual splitting parameters and associated errors at each station

Station Name	Event ID	Fast Angle	Fast Angle Error	Delay Time	Delay Time Error	Phase
AFFS	1323924	-2	4	2.25	0.35	SKS
AFFS	1329072	-12	10	1.65	0.20	SKS
AFFS	1329189	12	8	1.55	0.25	SKS
AFFS	1380219	-18	10	1.45	0.15	SKS
AFFS	1383781	-12	6	1.65	0.10	SKS
AFFS	1467351	-8	10	1.45	0.45	SKS
AFFS	1472424	-12	8	1.80	0.30	SKS
AFFS	1473169	-2	6	1.55	0.10	SKS
AFFS	1551781	-8	6	0.90	0.10	S
AFFS	1552135	-40	20	0.55	0.10	S
AFFS	1592364	2	4	2.05	0.20	SKKS
AFFS	4208653	20	12	1.70	0.45	SKKS
AFFS	4259018	-18	18	1.20	0.25	SKS
AFFS	4473144	4	18	1.15	0.20	SKS
AFFS	4589632	-8	18	1.10	0.40	S
AFIF	714751	-34	10	0.95	0.15	SKS
AFIF	715737	-6	24	1.25	1.10	SKS
AFIF	719689	-8	24	1.25	0.30	SKS
AFIF	720054	0	22	1.30	0.40	SKS
AFIF	720105	-20	18	1.55	0.35	SKS
AFIF	720171	-18	2	1.45	0.05	SKS
AFIF	720923	0	18	1.35	0.80	SKS
AFIF	722399	-4	16	1.00	0.35	SKS
AFIF	722782	-14	12	1.35	0.20	SKS
AFIF	722827	-18	4	1.55	0.10	SKS
AFIF	722931	-22	8	1.50	0.10	SKS
AFIF	724135	-16	14	1.15	0.15	SKS
AFIF	724503	-22	4	1.45	0.10	SKS
AFIF	733206	0	6	2.20	0.40	SKS
ALWS	1321048	2	16	1.85	0.75	S
ALWS	1470690	6	2	2.00	0.15	SKS
ALWS	1472424	2	10	1.60	0.15	SKS
ALWS	1581565	20	12	0.90	0.10	S
ALWS	1592364	-10	10	1.85	0.35	SKKS
ALWS	4207220	-6	14	1.20	0.30	S

ALWS	4208653	0	6	1.75	0.30	SKS
ALWS	4473144	12	6	1.55	0.25	SKS
ALWS	4473481	0	12	1.00	0.20	SKS
ARSS	1589036	12	8	1.25	0.50	SKS
ARSS	1591203	0	20	1.05	0.55	SKS
ARSS	3992367	-4	8	1.05	0.45	SKS
ARSS	4208653	8	6	0.75	0.15	SKS
ARSS	4473144	0	6	0.95	0.05	SKS
ARSS	4596577	34	20	1.70	0.45	S
AYUS	1330394	-2	8	2.10	0.60	SKS
AYUS	1330404	-14	18	1.85	0.50	S
AYUS	1380430	14	4	1.60	0.30	SKS
AYUS	1380683	38	8	2.50	0.05	SKS
AYUS	1381176	0	22	1.15	0.35	SKS
AYUS	1470690	4	10	1.50	0.25	SKS
AYUS	1472424	4	10	1.30	0.10	SKS
AYUS	1554837	16	18	1.35	0.30	SKKS
AYUS	1562488	-28	12	0.85	0.20	S
AYUS	1581565	-2	6	0.85	0.05	S
AYUS	1589036	0	10	1.80	0.45	SKS
AYUS	1590598	14	12	1.55	0.20	SKKS
AYUS	1591203	0	14	1.15	0.30	SKS
AYUS	4207220	-14	6	1.30	0.15	S
AYUS	4351768	-2	8	2.10	0.55	SKS
AYUS	4473144	16	6	1.35	0.20	SKS
BDAS	1325258	2	6	1.65	0.20	SKS
BDAS	1327660	10	4	1.60	0.05	SKS
BDAS	1329189	2	6	1.65	0.35	SKS
BDAS	1330394	-8	10	1.80	0.75	SKS
BDAS	1378170	10	4	1.75	0.15	S
BDAS	1378782	-6	6	2.05	0.20	SKS
BDAS	1380430	10	6	2.45	0.70	SKS
BDAS	1383781	-2	6	1.55	0.05	SKS
BDAS	1385516	10	8	1.85	0.65	SKS
BDAS	1467351	6	20	1.45	0.30	SKS
BDAS	1469289	8	16	1.20	0.30	SKS
BDAS	1472424	10	4	1.50	0.05	SKS
BDAS	1494829	0	8	2.50	0.20	SKS
BDAS	1580135	18	8	1.55	0.20	SKS
BDAS	1591203	2	12	1.45	0.35	SKS

BDAS	3991754	-26	24	1.15	0.40	SKKS
BDAS	4062674	0	6	1.95	0.15	SKS
BDAS	4078622	10	4	1.60	0.05	SKS
BDAS	4207220	-8	8	1.35	0.25	S
BDAS	4208653	12	10	1.85	0.40	SKS
BDAS	4351768	-8	18	1.80	1.00	SKS
BDAS	4596577	-10	8	1.75	0.15	S
BLJS	1383781	2	8	1.30	0.20	SKS
BLJS	1582417	-38	18	0.90	0.75	S
BLJS	4205566	24	18	0.55	0.20	SKS
BLJS	4409772	-2	18	1.00	0.30	SKS
BLJS	4473144	-2	10	1.30	0.25	SKS
DJNS	1473169	-18	14	1.10	0.15	SKS
DJNS	1551781	-20	8	1.70	0.20	S
DJNS	1562488	-6	14	2.35	0.35	S
DJNS	1580135	-6	14	1.45	1.00	SKS
DJNS	1581565	4	20	0.80	0.20	S
DJNS	4207220	-16	10	2.50	0.20	S
DJNS	4208653	-4	8	0.70	0.05	SKS
HALM	714489	18	6	1.00	0.35	SKS
HALM	720105	2	14	1.05	0.40	SKS
HALM	720110	-14	12	0.70	0.15	SKS
HALM	720171	-20	8	0.70	0.10	SKS
HALM	721404	22	22	1.50	0.65	SKS
HALM	722399	-14	8	0.65	0.05	SKS
HALM	722782	-2	10	0.85	0.30	SKS
HALM	722931	-4	16	1.00	0.30	SKS
HALM	724135	4	24	0.55	0.15	SKS
HALM	724225	10	16	1.00	0.25	SKS
HALM	725459	-28	22	0.85	0.25	SKS
HALM	726020	2	22	1.00	0.35	SKS
HALM	733206	6	8	1.70	0.60	SKS
HAQS	1327660	4	20	1.55	0.30	SKS
HAQS	1378170	14	4	1.90	0.25	S
HAQS	1378658	8	20	2.05	0.80	SKS
HAQS	1380392	2	6	1.80	0.50	S
HAQS	1380430	24	4	1.20	0.30	SKS
HAQS	1380967	26	20	1.05	0.85	S
HAQS	1469289	18	14	1.30	0.15	SKS
HAQS	1472424	0	8	1.60	0.15	SKS

HAQS	1552306	20	4	1.80	0.45	SKS
HAQS	3991464	32	16	1.60	0.55	SKS
HAQS	4078622	4	22	1.70	0.30	SKS
HAQS	4208653	0	24	1.25	0.50	SKS
HAQS	4474575	-2	20	2.45	0.35	SKS
HAQS	4540559	-2	22	1.25	0.30	SKS
HASS	1329072	-32	6	0.75	0.10	SKS
HASS	1330394	0	4	1.70	0.35	SKS
HASS	1378170	10	2	1.70	0.40	S
HASS	1380430	-10	4	0.85	0.10	SKS
HASS	1381291	16	6	1.50	0.25	S
HASS	1470597	-18	12	0.85	0.15	SKS
HASS	1562488	-32	20	0.80	0.30	S
HASS	1580135	-16	2	0.90	0.10	SKS
HASS	1592364	2	14	1.50	0.35	SKS
HASS	4473144	4	6	1.40	0.10	SKS
HASS	4589463	-12	8	2.25	0.10	S
HASS	4590172	6	6	0.95	0.15	S
HASS	4595874	-22	14	1.30	0.25	S
HILS	1329189	-12	2	1.80	0.15	SKS
HILS	1380392	-30	18	0.95	0.30	S
HILS	1382484	-8	6	1.00	0.15	SKS
HILS	1472392	-6	16	1.40	0.35	SKKS
HILS	1473169	-26	20	1.25	0.30	SKS
HILS	4208653	-26	12	1.00	0.15	SKS
HILS	4473144	-28	8	0.95	0.15	SKS
HILS	4473481	0	18	0.95	0.25	SKS
HIT	757685	10	4	1.75	0.40	SKS
HIT	763405	20	4	1.35	0.15	SKS
HIT	766330	18	6	1.35	0.20	SKS
HIT	1382400	8	10	1.10	0.10	SKS
HIT	1441489	-14	12	2.40	0.75	SKS
HIT	1467240	6	12	2.00	1.10	S
HIT	1467351	-2	22	1.15	0.20	SKS
HIT	1471587	6	16	1.00	1.50	SKS
JMOS	1327281	8	8	2.40	0.55	SKS
JMOS	1378658	6	10	2.00	0.50	SKS
JMOS	1467351	-4	6	1.70	0.15	SKS
JMOS	1470690	14	4	1.80	0.25	SKS
JMOS	1472392	14	12	1.65	0.85	SKS

JMOS	1472424	-6	6	1.65	0.10	SKS
JMOS	1473169	0	6	1.10	0.25	SKS
JMOS	1580135	4	6	1.90	0.30	SKS
JMOS	1592364	-4	8	1.20	0.10	SKKS
JMOS	4207220	-8	10	1.00	0.15	S
JMOS	4208653	-2	6	1.60	0.30	SKS
JMOS	4259018	2	6	1.70	0.25	SKS
JMOS	4268963	10	18	1.60	0.50	SKKS
JMOS	4473144	2	14	1.65	0.75	SKS
JMOS	4540559	10	16	1.15	0.15	SKS
KBRS	1383781	10	8	1.70	0.10	SKS
KBRS	1472424	0	4	1.40	0.10	SKS
KBRS	1473169	-18	22	0.95	0.30	SKS
KBRS	1582417	-28	12	1.15	0.30	S
KBRS	4208653	-4	14	1.30	0.20	SKS
KBRS	4259018	2	14	1.00	0.25	SKS
KBRS	4268963	14	6	2.00	0.30	SKS
LTHS	1329189	2	6	1.10	0.15	SKS
LTHS	1383781	-2	12	1.10	0.20	SKS
LTHS	1471662	-24	16	1.30	0.15	SKS
LTHS	1472246	6	20	1.85	0.40	SKS
LTHS	1472424	6	6	1.20	0.05	SKS
LTHS	4259018	-30	20	0.75	0.15	SKS
LTHS	4567778	-20	22	1.30	0.30	SKS
NAMS	1321048	-26	4	1.70	0.15	S
NAMS	1327660	10	6	1.20	0.20	SKS
NAMS	1329189	6	6	1.35	0.15	SKS
NAMS	1330394	4	6	1.50	0.40	SKS
NAMS	1330404	-22	24	1.10	0.30	S
NAMS	1378782	0	12	1.15	0.35	SKS
NAMS	1380967	-36	20	1.45	0.50	S
NAMS	1381291	2	10	1.75	0.75	S
NAMS	1383781	4	6	1.15	0.10	SKS
NAMS	1471801	-18	14	1.30	0.15	SKS
NAMS	1472392	4	24	1.00	0.55	SKS
NAMS	1472424	12	14	1.45	0.30	SKS
NAMS	1473169	-4	8	1.10	0.10	SKS
NAMS	1552135	0	18	1.55	0.70	S
NAMS	4078622	10	4	1.25	0.15	SKS
NAMS	4351768	4	4	1.55	0.25	SKS

QURS	1326192	6	10	1.05	0.15	SKS
QURS	1327660	-8	6	1.40	0.30	SKS
QURS	1329189	2	4	1.45	0.05	SKS
QURS	1378782	-4	8	1.80	0.35	SKS
QURS	1382484	-22	24	0.40	0.10	SKS
QURS	1467351	2	8	1.30	0.30	SKS
QURS	1472424	-8	6	1.40	0.25	SKS
QURS	1473169	4	10	2.10	0.35	SKS
QURS	1551781	-38	24	0.45	0.10	SKS
QURS	4078622	-8	10	1.40	0.50	SKS
QURS	4268963	8	6	1.70	0.50	SKS
RANI	714828	40	20	1.15	0.15	S
RANI	718052	4	6	2.25	1.15	SKS
RANI	719689	22	24	1.90	1.15	SKS
RANI	720054	0	16	1.25	0.30	SKS
RANI	720105	-10	8	1.30	0.35	SKS
RANI	720171	-2	8	1.45	0.30	SKS
RANI	720923	4	4	2.00	0.25	SKS
RANI	721404	2	2	1.90	0.40	SKS
RANI	721507	0	10	2.10	1.10	SKS
RANI	722782	8	8	1.20	0.20	SKS
RANI	722931	6	8	1.80	0.40	SKS
RAYN	000512	4	16	1.15	0.35	SKS
RAYN	010705	42	16	1.00	0.20	SKS
RAYN	021012	12	6	1.30	0.25	SKS
RAYN	021112	8	24	0.45	0.15	SKS
RAYN	050613	8	14	1.25	0.30	SKS
RAYN	717753	16	18	0.95	0.30	SKS
RAYN	717994	4	4	1.85	0.70	SKS
RAYN	720100	0	4	1.10	0.15	SKS
RAYN	720171	2	10	0.90	0.30	SKS
RAYN	721264	12	4	1.20	0.35	SKS
RAYN	960819	4.2	16	1.18	0.55	SKS
RAYN	970720	2	14	1.30	0.30	SKS
RAYN	970727	-20	4	1.90	0.50	SKS
RAYN	971217	-10	10	0.75	0.15	SKS
RAYN	971222	12	6	1.10	0.40	SKS
RAYN	980130	4	14	1.25	0.40	SKS
RIYD	724503	6	6	0.70	0.10	SKS
RIYD	724537	34	10	2.05	0.85	S

RIYD	727822	-16	4	1.05	0.15	S
RIYD	728015	-12	12	2.10	0.25	S
RIYD	731866	-36	6	1.20	0.15	S
RIYD	733206	60	18	0.65	0.20	SKS
RIYD	734243	-8	24	2.15	1.60	S
RUW	1380389	-10	12	1.35	0.20	S
RUW	1383840	6	20	1.30	0.95	SKS
RUW	1383841	6	10	1.25	0.70	SKS
SODA	714489	-8	8	1.10	0.35	SKS
SODA	715737	-6	6	1.55	0.65	SKS
SODA	717753	-6	14	1.90	0.15	SKS
SODA	718511	-16	6	1.40	0.10	SKS
SODA	720105	-10	4	1.25	0.10	SKS
SODA	720171	-12	8	1.35	0.15	SKS
SODA	723739	-4	14	1.30	0.35	SKS
SODA	724225	-4	4	1.60	0.15	SKS
SODA	724503	-8	22	1.40	0.60	SKS
SODA	725459	-22	22	1.75	0.20	SKS
SODA	726575	-8	6	1.80	0.65	SKS
SODA	728981	-16	20	1.10	0.40	SKS
SODA	732743	24	24	2.00	0.55	SKS
SODA	733206	-4	4	1.65	0.35	SKS
TAIF	722827	0	14	1.15	0.55	SKS
TAIF	723086	0	8	1.50	0.05	SKS
TAIF	723739	12	6	1.40	0.15	SKS
TAIF	723955	2	16	1.10	0.35	SKS
TAIF	724225	16	10	1.00	0.15	SKS
TAIF	724503	22	6	1.10	0.10	SKS
TATS	1327660	-4	12	1.80	0.55	SKS
TATS	1383781	-6	8	1.65	0.20	SKS
TATS	1467351	-4	16	2.05	0.90	SKS
TATS	1467512	10	20	2.00	0.80	SKS
TATS	1471801	2	10	1.50	0.15	SKS
TATS	1472424	-4	4	1.65	0.10	SKS
TATS	1473169	-16	10	1.45	0.20	SKS
TATS	1582417	14	16	1.10	0.30	S
TATS	4208653	-16	8	0.65	0.05	SKS
TAYS	1327281	14	6	2.25	0.40	SKS
TAYS	1327660	12	8	1.75	0.15	SKS
TAYS	1329072	16	16	1.45	0.50	SKS

TAYS	1329189	8	16	1.50	0.70	SKS
TAYS	1330394	-4	20	1.85	0.85	SKS
TAYS	1378170	12	2	2.00	0.15	S
TAYS	1378658	8	8	1.90	0.45	SKS
TAYS	1380392	2	4	1.75	0.35	SKKS
TAYS	1380430	14	6	2.40	0.75	SKS
TAYS	1383781	8	10	1.75	0.15	SKS
TAYS	1467351	10	8	1.85	0.20	SKS
TAYS	1472392	-10	12	2.45	0.70	SKS
TAYS	4078622	12	6	1.75	0.15	SKS
TAYS	4208653	8	6	1.50	0.30	SKS
TAYS	4405407	2	20	1.70	0.30	SKS
TBKS	1327660	-8	4	1.10	0.10	SKS
TBKS	1329189	10	20	0.75	0.25	SKKS
TBKS	1330404	-32	24	0.60	0.35	S
TBKS	1383822	-12	8	1.50	0.50	SKKS
TBKS	1472424	-10	6	1.25	0.15	SKS
TBKS	1582417	-38	8	1.40	0.15	S
TBKS	4078622	-6	4	1.05	0.15	SKS
TBKS	4596577	-10	10	2.05	0.10	S
UQSK	722931	0	6	1.45	0.25	SKS
UQSK	724225	-6	10	1.45	0.20	SKS
UQSK	724503	-2	10	1.35	0.50	SKS
UQSK	724508	-2	24	1.15	0.45	SKS
UQSK	726020	-12	12	1.50	0.50	SKS
UQSK	726645	18	12	2.15	0.55	SKS
UQSK	732743	-16	18	1.15	0.55	SKS
UQSK	732949	10	16	1.10	0.15	S
UQSK	733206	-8	2	1.80	0.25	SKS
YNBS	1327660	-6	4	1.35	0.15	SKS
YNBS	1378170	12	8	1.65	0.70	S
YNBS	1472424	2	6	1.30	0.10	SKS
YNBS	1473169	-2	8	1.55	0.20	SKS
YNBS	1582417	-30	18	1.55	0.80	S
YNBS	4078622	-6	4	1.50	0.15	SKS
YNBS	4259018	0	10	1.35	0.20	SKS

Table DR3. Average splitting parameters and associated standard deviations at each station

Station Name	Latitude	Longitude	Avg. Fast Angle	Fast Angle St. Dev	Avg. Delay Time	Delay Time St. Dev.
AFFS	23.927	43.001	-6.80	14.02	1.466	0.44
AFIF	23.931	43.040	-13.00	10.28	1.378	0.30
ALWS	29.310	35.065	2.89	9.01	1.522	0.40
ARSS	25.881	43.237	8.33	13.88	1.124	0.33
AYUS	28.189	35.269	2.75	15.16	1.518	0.46
BDAS	28.432	35.101	1.91	10.02	1.702	0.34
BLJS	19.881	41.599	-3.20	22.25	1.010	0.31
DJNS	17.707	43.543	-9.43	8.77	1.514	0.71
HALM	22.845	44.320	-1.38	14.54	0.966	0.33
HAQS	29.055	34.930	10.57	11.57	1.608	0.38
HASS	25.190	49.694	-8.00	15.64	1.266	0.46
HILS	27.384	41.792	-17.00	11.76	1.162	0.31
HIT	32.475	38.402	6.50	10.84	1.512	0.49
JMOS	29.169	35.109	3.07	7.12	1.606	0.37
KBRS	25.789	39.262	-3.43	14.96	1.358	0.38
LTHS	20.275	40.411	-8.86	15.32	1.228	0.33
NAMS	19.171	42.208	-3.12	14.34	1.346	0.23
QURS	31.386	37.324	-6.00	13.65	1.314	0.52
RANI	21.312	42.780	6.73	13.51	1.664	0.40
RAYN	23.522	45.500	6.26	12.98	1.164	0.36
RIYD	24.722	46.640	4.00	32.76	1.414	0.67
RUW	29.743	35.841	0.67	9.23	1.300	0.05
SODA	18.292	42.380	-7.14	10.43	1.510	0.29
TAIF	21.281	40.350	8.67	9.35	1.208	0.20
TATS	19.541	43.478	-2.67	10.20	1.538	0.44
TAYS	28.551	34.872	7.47	7.19	1.856	0.31
TBKS	28.225	36.549	-13.25	15.15	1.212	0.45
UQSK	25.789	42.360	-2.00	10.58	1.456	0.34
YNBS	24.340	37.992	-4.29	12.88	1.464	0.13

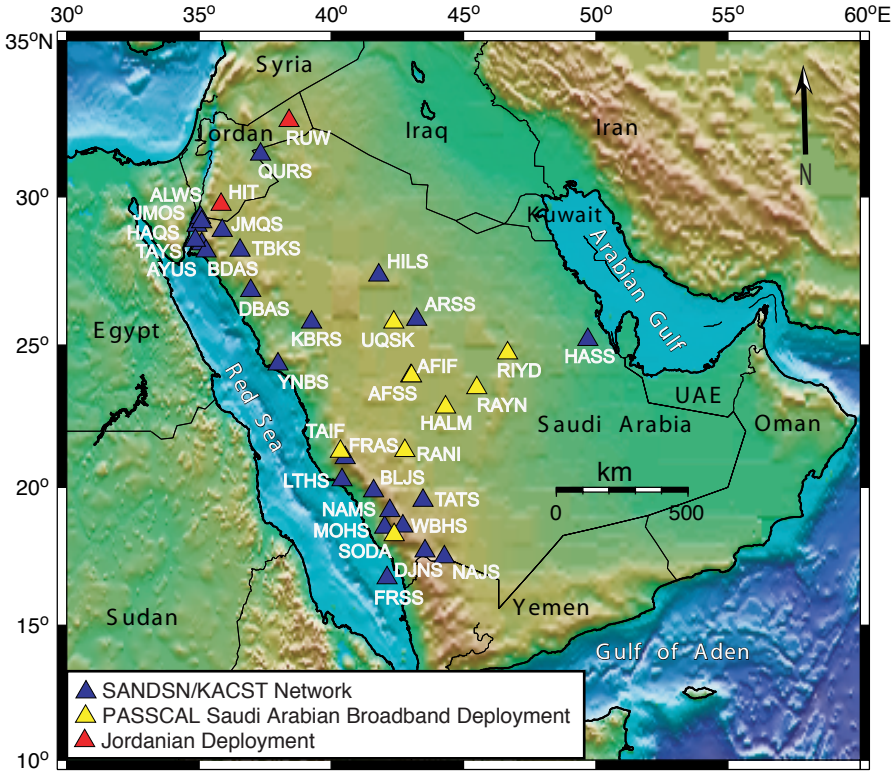
30°
35°
40°
45°
50°
55°
60°E
35°N
30°
25°
20°
15°
10°
Syria
Jordan
Iraq
Iran
Kuwait
Arabian Gulf
Egypt
Red Sea
Saudi Arabia
UAE
Oman
Yemen
Sudan
Gulf of Aden
N
km
0
500
RUW
QURS
HIT
ALWS
JMOS
HAQS
TAYS
AYUS
JMQS
TBKS
BDAS
DBAS
HILS
ARSS
KBRS
UQSK
HASS
RIYD
AFIF
YNBS
AFSS
RAYN
HALM
TAIF
FRAS
RANI
LTHS
BLJS
TATS
NAMS
MOHS
WBHS
SODA
DJNS
NAJS
FRSS
SANDSN/KACST Network
PASSCAL Saudi Arabian Broadband Deployment
Jordanian Deployment

Figure DR1.

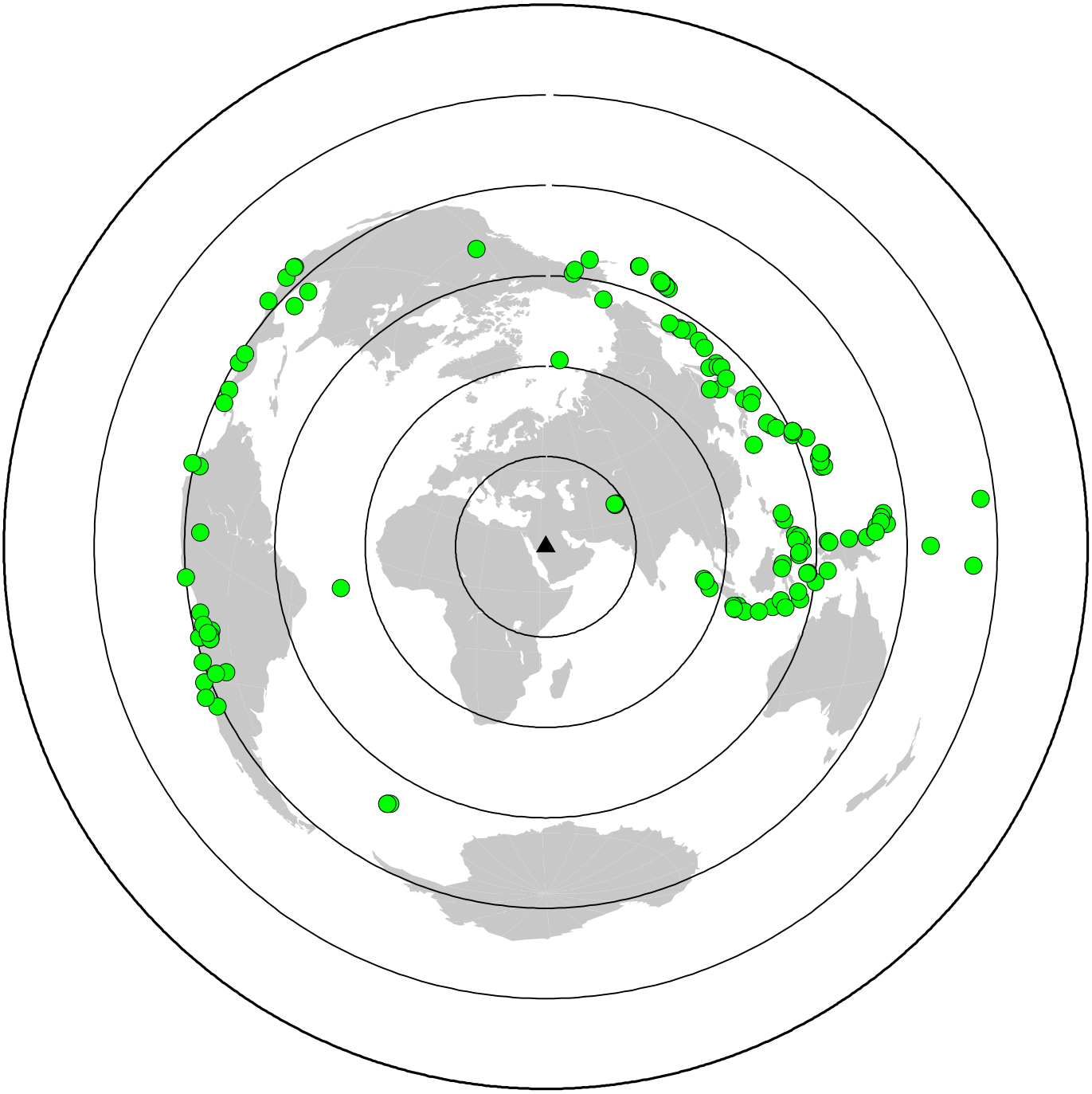

Figure DR2.

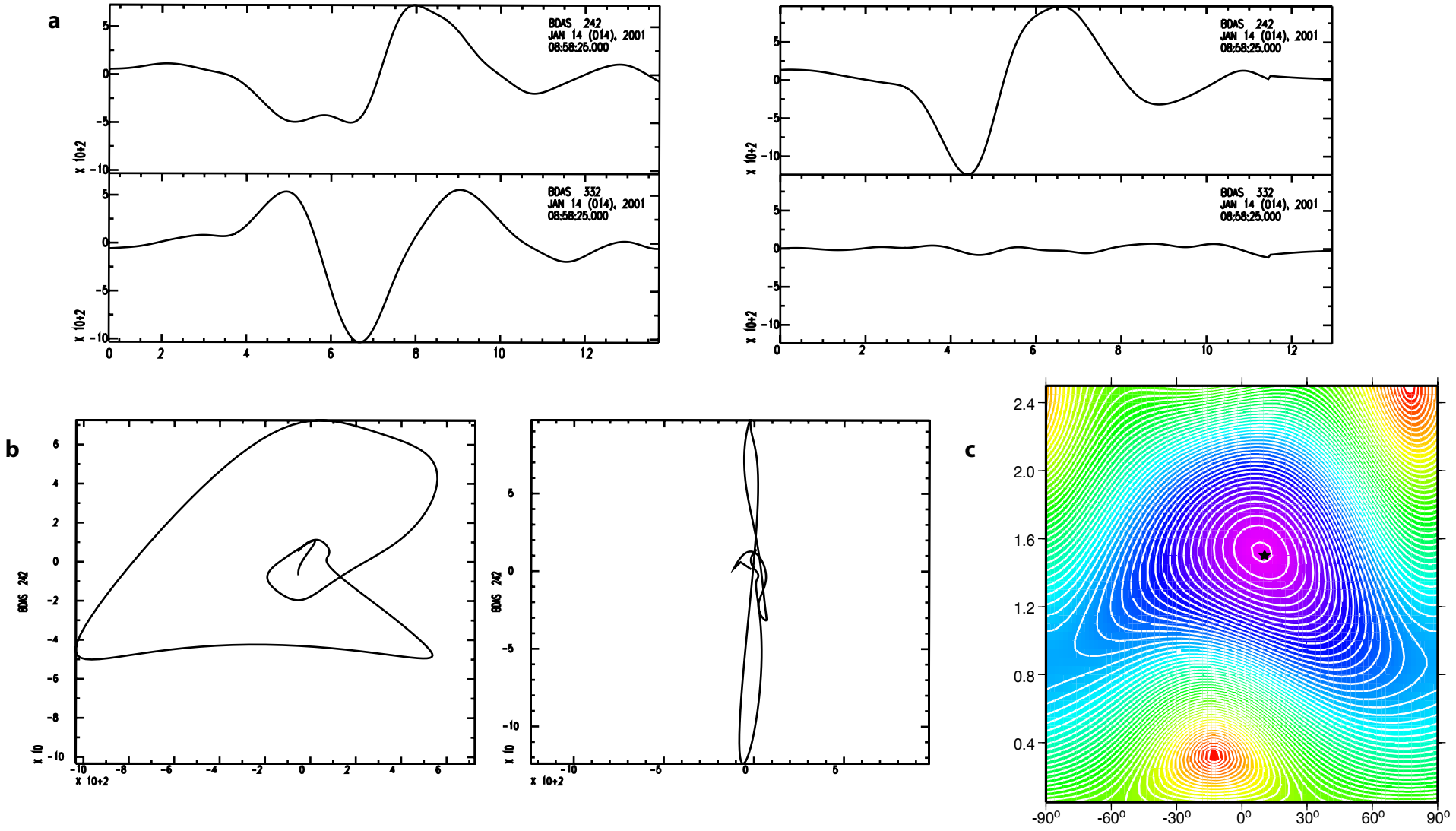
a
BDAS 242
JAN 14 (014), 2001
08:58:25.000
BDAS 332
JAN 14 (014), 2001
08:58:25.000
x 10+2
b
BDAS 242
x 10
x 10+2
c
2.4
2.0
1.6
1.2
0.8
0.4
-90°
-60°
-30°
0°
30°
60°
90°

Figure DR3.

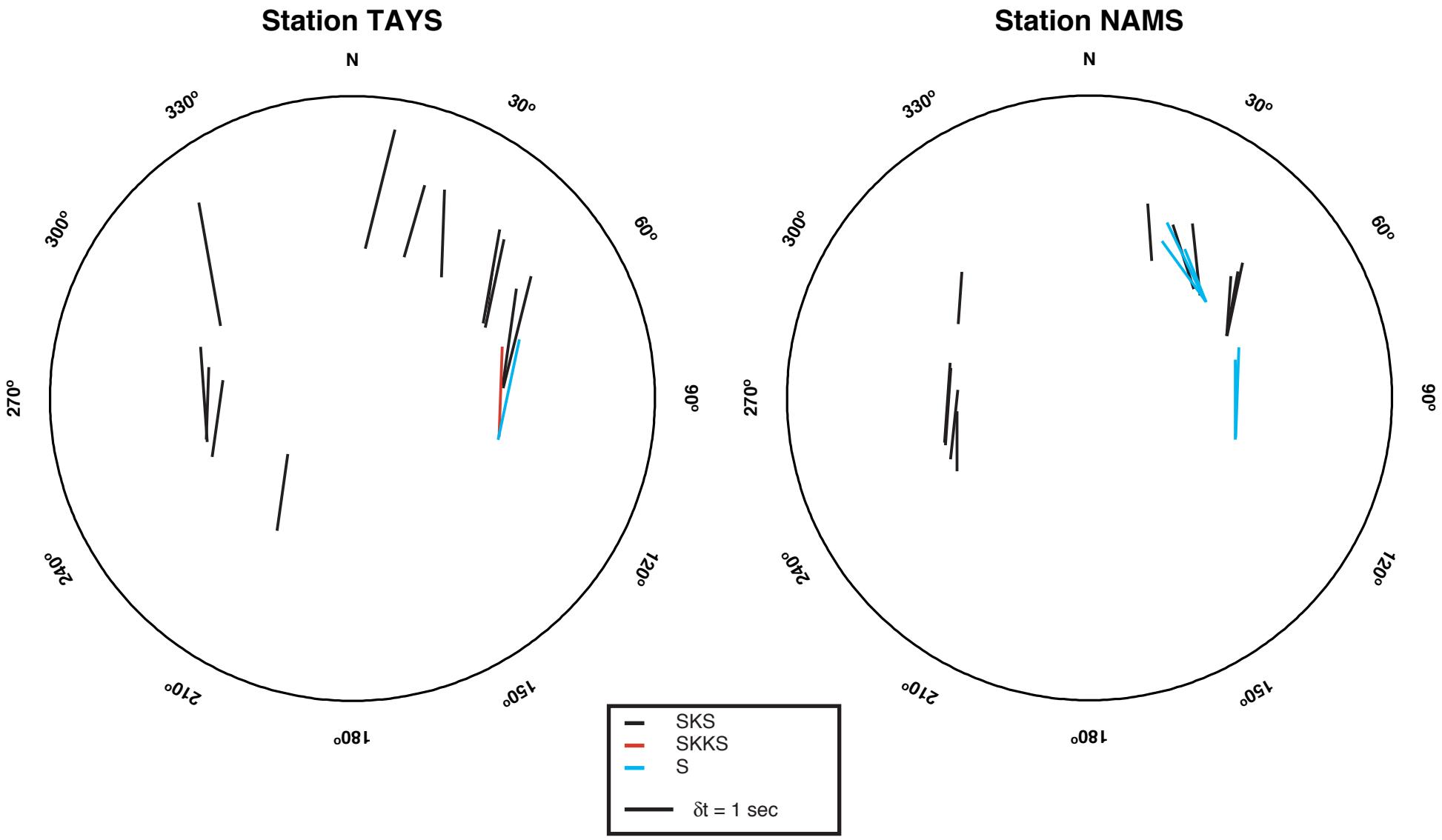
Station TAYS
Station NAMS
N
30°
60°
90°
120°
150°
180°
210°
240°
270°
300°
330°
SKS
SKKS
S
δt = 1 sec

Figure DR4.